Published in final edited form as:
Ultrasonics. 2014 January ; 54(1): 177–186. doi:10.1016/j.ultras.2013.06.008.

Monitoring tissue inflammation and responses to drug treatments in early stages of mice bone fracture using 50 MHz ultrasound

Yen-Chu Chen[a], **Yi-Hsun Lin**[b], **Shyh-Hau Wang**[b,c], **Shih-Ping Lin**[d], **K. Kirk Shung**[e], and **Chia-Ching Wu**[a,c,d,*]

[a]Department of Cell Biology & Anatomy, National Cheng Kung University, Tainan 701, Taiwan

[b]Department of Computer Science and Information Engineering, National Cheng Kung University, Tainan 701, Taiwan

[c]Medical Device and Innovation Center, National Cheng Kung University, Tainan 701, Taiwan

[d]Department of Biomedical Engineering, National Cheng Kung University, Tainan 701, Taiwan

[e]Department of Biomedical Engineering, University of Southern California, Los Angeles, CA 90089, USA

Abstract

Bone fracture induces moderate inflammatory responses that are regulated by cyclooxygenase-2 (COX-2) or 5-lipoxygenase (5-LO) for initiating tissue repair and bone formation. Only a handful of non-invasive techniques focus on monitoring acute inflammation of injured bone currently exists. In the current study, we monitored *in vivo* inflammation levels during the initial 2 weeks of the inflammatory stage after mouse bone fracture utilizing 50 MHz ultrasound. The acquired ultrasonic images were correlated well with histological examinations. After the bone fracture in the tibia, dynamic changes in the soft tissue at the medial-posterior compartment near the fracture site were monitored by ultrasound on the days of 0, 2, 4, 7, and 14. The corresponding echogenicity increased on the 2nd, 4th, and 7th day, and subsequently declined to basal levels after the 14th day. An increase of cell death was identified by the positive staining of deoxynucleotidyl transferase dUTP nick end-labeling (TUNEL) assay and was consistent with ultrasound measurements. The increases of both COX-2 and Leukotriene B4 receptor 1 (BLT_1, 5-LO-relative receptor), which are regulators for tissue inflammation, in the immunohistochemistry staining revealed their involvement in bone fracture injury. Monitoring the inflammatory response to various non-steroidal anti-inflammatory drugs (NSAIDs) treatments was investigated by treating injured mice with a daily oral intake of aspirin (Asp), indomethacin (IND), and a selective COX-2 inhibitor (SC-236). The Asp treatment significantly reduced fracture-increased echogenicity (hyperechogenicity, $p < 0.05$) in ultrasound images as well as inhibited cell death, and expression of COX-2 and BLT_1. In contrast, treatment with IND or SC-236 did not reduce the hyperechogenicity, as confirmed by cell death (TUNEL) and expression levels of COX-2 or BLT_1.

*Corresponding author. Address: No. 1, University Rd., Tainan, Taiwan. Tel.: +886 6 2353535×5327; fax: +886 6 2093007. joshccwu@mail.ncku.edu.tw (C.-C. Wu).

Taken together, the current study reports the feasibility of a noninvasive ultrasound method capable of monitoring post-fracture tissue inflammation that positively correlates with histological findings. Results of this study also suggest that this approach may be further applied to elucidate the underlying mechanisms of inflammatory processes and to develop therapeutic strategies for facilitating fracture healing.

Keywords

50 MHz ultrasound; Echogenicity; Inflammation; Fracture; NSAIDs

1. Introduction

The present study utilized an ultrasound at a center frequency close to 50 MHz to monitor tissue structural changes during the early stage of bone fracture in mice by correlating results to those of histologically changes. Bone fracture is a medical complication resulting from a break in the continuity of bone typically caused by high force impacts or stress. The healing process of bone fracture can be divided into inflammation, soft callus formation, hard callus formation, and remodeling stages [1,2]. Fracture may immediately disrupt blood vessels and cause hematoma, which contains immune cells from peripheral blood or bone marrow at the fracture site. Prior to bone regeneration, the surrounding inflammatory cells and bone/cartilage progenitor cells produce pro-inflammatory protein molecules during the inflammation stage to regulate and trigger fracture repair [3–5].

Bone fracture normally is healed by inducing the cyclooxygenase (COX) signaling pathway to trigger an inflammatory response, particularly the release of specific lipid compounds called prostaglandins. This process regulates both the bone resorption by osteoclasts and new bone formation by osteoblasts [4]. The inflammatory responses induced via COX and/or 5-lipoxygenase (5-LO) signal pathway play important roles in bone regeneration. Although tissue inflammation is important for fracture healing, it also induces pain, fever, and swelling complications in the injured tissue [6]. COX-2 is an enzyme of COX family and can convert arachidonic acid (AA) to prostaglandin E2 (PGE_2) for regulating inflammatory responses and pain signals in peripheral tissues [7]. However, the AA can also be converted into a different inflammatory factor named leukotriene by an enzyme called the 5-lipoxygenase (5-LO) [8,9]. The counterbalance between COX-2 and 5-LO indicates a complex network that is altered by the activities of various enzymes during bone fracture healing [10,11]. Inflammatory responses can be inhibited by steroid drug, such as dexamethasone, but some side effects common to systemic glucocorticoids may occur over a period of more than a few days. The non-steroidal anti-inflammatory drugs (NSAIDs) are commonly given to reduce pain and inflammation by inhibiting COX [12]. Common NASIDs, such as Aspirin (Asp), indomethacin (IND), and selective COX inhibitor, are classified based on their chemical structure or mechanism of action. Conversely, numerous studies report that the treatment with IND, a nonselective COX inhibitor, tends to impair the fracture healing process and increase the risk of developing a non-union lesion [12–15]. The aforementioned inflammation inhibitors may have a critical influence on fracture healing, but their responses during drug treatments are still poorly understood.

The detection of tissue inflammation in a fractured bone will not only aid in the determination of the healing progress, but also provide suggestions for treatment strategy. Currently, there are only a handful of non-invasive techniques able to monitor the injured bone to study the corresponding acute inflammation. Infrared thermal imaging is capable of measuring the skin temperature to reflect the degree of inflammation in disease tissues [16]. However, the thermal image can only detect superficial inflammatory responses in the tissue under the skin surface. Magnetic resonance imaging (MRI) is another remarkable technique that has been documented to monitor inflammation in human muscle tissue. This is executed by observing the active phase with images formed by Short TI Inversion Recovery (STIR) and fat-saturated gadolinium-enhanced spin-lattice relaxation time (T1-weighted) [17]. However, MRI remains cost ineffective and is highly time-consuming for imaging. On the other hand, ultrasound, which has been frequently applied to clinical diagnosis, has the advantages of low-cost, wide availability, portability, and noninvasiveness. Although the echogenicity of ultrasound image is resultant from the anatomy and acoustic properties of the tissue [18], it still relies heavily on operator's skill to better discern the acquired ultrasound image for characterizing tissue properties and the significance of the observed variations. To alleviate these issues, several statistical models were proposed and implemented in an attempt to further quantitatively characterize tissue properties using ultrasonic signals backscattered from biological tissues [19]. Among those statistical models, the Nakagami statistics is a general model with relatively less computational complications [19]. Moreover, to further improve the resolution of ultrasonic images, the employed frequency needs to be readily increased. For instance, as the frequency was increased above 15 MHz, the corresponding ultrasound image resolution was increased to less than 0.1 mm [20]. Ultrasounds with frequencies between 30 and 50 MHz have been used for ophthalmology, dermatology, and small animal studies [21]. As the ultrasound frequencies were further increased to 200 MHz, the corresponding axial and lateral resolutions respectively approached 14 and 12 μm, and the acquired images from eye and skin tissues correlated well to histological results [22]. Due to pulse-echo technique is typically applied for ultrasound image formation, the temperature of the interface between the soft tissue and skull of a mice did not apparently rise after response to the insonation of a 40 MHz ultrasound for 3 min [23]. All of these observations suggest that high resolution ultrasound may be feasible for monitoring finer structural changes of tissues associated with bone fracture healing. Beside the commercially available 50 MHz ultrasound small animal scanner, such as VisualSonics, we are interested to correlate the ultrasound images with histological structures which require the automatic serial scanning of ultrasound transducer on the anatomical planes. We hypothesize that inflammation in living animals can be detected *in vivo* by ultrasound images, and that inflammation is quantifiable by acoustic parameters associated with echogenicity or Nakagami statistical analysis. An ultrasound system with the a center frequency near 50 MHz was utilized to image anatomical structures *in vivo* in mice during the early stage of bone fracture. The results acquired from ultrasound images are capable of providing an overview of both soft and hard tissues with correlation to those of histological changes.

2. Methods

2.1. Fracture model in mice

The fracture model for investigating different healing progresses in mice was performed following the previously described procedure [24]. This does not require a complex fixation surgery on the mouse tibia to open a large wound. This procedure only requires the insertion of a steel pin for immobilizing the fractured bone around knee. Thus, tissue remodeling around the fracture site will directly reflect the normal healing processes without the influence of the surgical procedure itself. Briefly, the fracture model procedure begins with anesthetizing mice with chlorohydrate (0.04 g/ml in sterile phosphate buffered saline) (Sigma, USA), and then a closed fracture is produced in the diaphysis of the left hind tibia. An incision in the skin of the lateral knee was made and a 0.45 mm hole was drilled on the lateral condyle of the tibia. A steel pin (0.20 mm diameter) was inserted into the intramedullary canal of the tibia to stabilize the fractured bone. The mouse skin was marked to identify the alignment and the midpoint of the tibia. A vertical impact force (5.15×10^{-1} N) was applied using a free-dropping impacted-injury simulator (Fig. 1A) in the middle of the tibia shaft. Immediately after injury, an X-ray image with a resolution of 17.2 μm per pixel was taken to verify the status of complete fracture (Fig. 1B). All mice utilized in this study were healthy as certified by the staff of the National Cheng Kung University (NCKU) Animal Center. Eight-week old female B6 (C57BL/6N) mice were used for the study of inflammatory responses in early bone fracture healing. A total number of eighteen animals (n = 18) supplied by NCKU Animal Center were subjected to bone fracture experiments and then randomly assigned to different drug treatment groups. Animals had free access to food and water, and lived under a controlled illumination cycle before and after injury. The experimental procedures used for this study were reviewed and approved by the Institutional Animal Care and Use Committee (IACUC) at NCKU.

2.2. Ultrasound system

The ultrasound system for imaging applications was developed for the generation and reception of ultrasound waves [19]. This system is comprised of a single-element ultrasound transducer of 48 MHz central frequency and 35 MHz bandwidth (−6 dB) (NIH Ultrasonic Transducer Resource Center, University of Southern California, USA). The transducer characteristics are given in Table 1. The transducer was driven by a monocycle generator (AVB2-TB-C, AVTECH Electrosystems Ltd., NY, USA). An electronic limiter (Matec Instruments Company, MA, USA) connected between the receiver and an amplifier (Model LN1000A, Amplifier Research, PA, USA) was used to protect the devices from damage. After amplification, received signals were filtered by a bandpass filter (Model BIF-50, Mini-Circuits, NY, USA) and then digitized by an 8-bits analog-to-digital converter (PXI 5152, National Instruments, TX, USA) at a 500 MHz sampling frequency. B-mode ultrasonic images were acquired using a swept scanning mode. Ultrasonic signals at different anatomical locations were obtained by translating the transducer mounted on an axis of a piezoceramic motor (HR8, Nanomotion Ltd., Yokneam, Israel). In addition, the transducer was able to flexibly move to two other directions controlled by the other two axes of stepping motors (CM1-C-17L30A, Cool Muscle, Osaka, Japan) and actuators (KR2602A, THK, Tokyo, Japan). All of these motor stages were controlled by a motor controller

(DMC-1842, Galil Motion Control Inc., California, USA). The program for both data acquisition and motor control was developed using LabVIEW software (National Instruments, TX, USA).

2.3. Scanning of ultrasonic images

To better monitor the dynamic changes of acoustic parameters corresponding to the healing process, ultrasound signals were collected from each experimental mouse subsequently on the 2, 4, 7, and 14 days post-fracture. An animal restraint was modified to permit the scanning of ultrasonic images to detect soft tissue inflammation in bone fractured mice. Anesthetized mice were confined by the custom-made plexiglass restrainer that was subsequently filled with saline solution (Fig. 1C). Several markers and the longitudinal axis of the tibia were labeled on the skin of mice. The radio-frequency (RF) signals of each scan line were collected. Each acquired B-mode image, with the size of 10 mm × 3.8 mm, was composed of 1000 A-lines at a 10 μm interval. The scanning along the longitudinal axis of the subject's tibia was implemented to acquire serial scanning images along the medial side of the mouse leg. Sections within a range of 5 mm proximal and distal to fracture sites were scanned with serial scanning at 50 μm intervals per step, and a total of 200 slides were collected in each scanning.

2.4. Ultrasound image processesing and analysis

The acquired RF signals were processed via a work flow sequence including band-pass filtering, envelope detection using Hilbert transform, and logarithmic compression. The B-mode image was formed by mapping the processed signals to 8-bits gray scale level. The time-gain compensation was not immediately implemented during ultrasound scanning to ensure consistent imaging conditions for subsequent data analysis. The region of interest (ROI) of each B-mode image was designated using Image J software (Image J, NIH). The ROI was within the focal zone of the transducer covering the soft tissue posteromedial to the tibia, on the medial side of the leg's posteromedial compartment. The locations of ROI at different time points were selected by correlating the ultrasound images to a reference anatomical position in which the upper surface of the tibia corresponded to a region with high brightness in the ultrasound image. Tissue variations within the ROI were then monitored. The echogenicity was defined by the mean value of gray scale in the ROI. The changes of gray-scale echogenicity were assessed from the images of fractured bone relative to those of the same animal before fracture was made. The distribution of ultrasonic backscattered envelopes might exhibit various probability density functions. This depends on the scatterer concentration and arrangement of the interrogated biological tissue and several statistics, including Rayleigh [25], Rician [26], K [27], homodyned K [28], generalized K [29], and Nakagami [30] distributions, had been modeled. Except for the Nakagami distribution, most of aforementioned models are either incapable of broadly characterizing all of signals received from different tissues or suffering from computational complications, and tend to confine their practical applications to clinical diagnosis [31]. Nakagami distribution is a general model able to cover features of all scattering conditions, including pre-Rayleigh, Rayleigh and post-Rayleigh distributions [30]. The backscattered envelope resulting from the scatterers of lower concentrations tends to exhibit as pre-Rayleigh distribution and that Nakagami parameter is smaller than 1 [31]. As the

interrogated medium with scatterers of sufficient higher concentrations, known as well developed, the corresponding backscattered envelope tends to be Rayleigh distributed and is with Nakagami parameter equal to 1. The post-Rayleigh distribution, with Nakagami parameter larger than 1, may apply to the resolution cell that consists of highly concentrated scatterers with randomly and periodically distributed components [30]. Consequently, in addition to echogenicity, the Nakagami statistics may be applied to characterize scattering properties of the injured bone tissues.

2.5. NSAID treatments

To investigate the impact of inflammation inhibitors on tissue healing and echogenicity, the mice were fed with inhibitors after the fracture was conducted [12]. Aspirin (Asp), also known as acetylsalicylic acid, is regularly used in clinics to reduce fever and inflammation. Asp inhibits COX-1 and modifies the enzymatic activity of COX-2 [32]. The Asp (Sigma, USA) was administered in normal saline at dosages of 100–400 mg kg^{-1} day^{-1}. A nonselective COX inhibitor, IND (Sigma, USA) that inhibits both COX-1 and COX- 2 activities, was administered at dosages of 1.5–2 mg kg^{-1} day^{-1}. The selective COX-2 inhibitor, SC-236 (Sigma, USA), was given at 3mg kg^{-1} day^{-1}. Since this study was interested in exploring acute inflammatory responses, the animals with NSAIDs treatments were sacrificed for histological analysis after the completion of ultrasound scanning on the seventh day post-fracture. The inflammatory responses near fractured sites associated with various NSAIDs treatments were studied by ultrasound on the 0th, 2nd, 4th and 7th day post-fracture.

2.6. Immunohistological assessments

After sacrificing the mice, the hind limbs were isolated and fixed with 10% neutral buffered formalin (Leica, Germany) for 24 h at 4 °C. The tissue samples were decalcified using decalcifying buffer (Lecia, Germany) for 4 h at 4 °C, dehydrated by sequential immersion in gradient ethanol baths, and then cleared with Xylene and finally embedded in paraffin. The histological slides were transversely sectioned, with 5 μm defined section thickness. The histology was correlated to the serial ultrasound images acquired from the tissues underneath the marked skin of living animals. Hematoxylin and eosin (H&E) stain was employed to observe tissue morphology. Briefly, the tissue sections were cleaned by xylene immersion to remove paraffin and then were rehydrated with an ethanol gradient and double distilled H_2O (ddH_2O). The tissue sections were stained with hematoxylin (Lecia, Germany) for 4 min and followed by eosin (Lecia, Germany) for 20 s. The stained samples were rinsed with tap water, dehydrated in gradient ethanol (EtOH), and then mounted using xylene gel (Sigma, USA).

The cell death (apoptosis) in the histological tissue was detected *in situ* by a commercial terminal deoxynucleotidyl transferase dUTP nick end-labeling (TUNEL) assay kit (Roche, Switzerland). The TUNEL assay was performed following the manufacturer's protocol. Briefly, the paraffin tissue sections were xylene cleaned, EtOH gradient rehydrated, and incubated with Proteinase K solution (Sigma, USA) for 30 min at 37 °C. The mixture of enzyme and labeled solution, at a ratio of 1:9, was applied to the samples for 60 min in the dark room at 37 °C. After rinsing twice with PBS, the converted-POD was added to the

samples for 30 min in the dark room at 37 °C. The 3,3′-Diaminobenzidine (DAB) (Dako, Carpinteria, CA, USA) was used to label the conjugated cells with brown coloring. TUNEL-positive cells will indicate DNA fragmentation during cell apoptosis. The tissue sections were counterstained with hematoxylin and stored in the mounting medium.

The immunohistochemistry (IHC) staining was performed to detect specific expression patterns of inflammatory proteins, including COX-2 and 5-LO. COX-2 is a key protein in the COX inflammation pathway, in which its expression levels were detected using primary antibodies specific against COX-2 (1:100, Cayman, USA). The Leukotriene B4 receptor 1 (BLT_1) antibody (1:100, Cayman, USA) relative to the 5-LO receptor was also used for high-affinity detection of the leukotriene B_4 expression levels. Briefly, paraffin sections were xylene de-waxed, EtOH gradient rehydrated, treated with 3% H_2O_2 (Sigma, USA) for 30 min and subsequently 0.25% Trypsin (Invitrogen, USA) for 20 min. Non-specific primary antibody binding was blocked by 5% fetal bovine serum (FBS, Invitrogen, USA) diluted in 0.02% Tris-buffered saline with tween 20 (TBST) (Sigma, USA). The tissue was incubated with primary antibody and stored overnight at 4 °C for inflammatory protein detection. After rinsing with 0.02% TBST, the primary antibodies were bound by secondary antibodies (1:500, abcam, UK) for 60 min and then labeled using AB reagent (Vector, USA) for 30 min to couple with DAB. Tissue sections were counterstained with hematoxylin and then mounted using mounting medium. The percentage of positive cells was calculated according to the number of positive nuclear stained cells and divided by the total cell number in the ROI where echogenicity quantification was carried out.

2.7. Statistical analysis

Data, calculated from the results of three independent animals for each time point from each treatment group, are presented as mean ± standard deviation (SD). The C57BL/6N age-matched mice obtained from the National Animal Institute were used to ensure similar physiological conditions. Each batch of mice were fractured, treated with different drugs, and then harvested at the same time to minimize experimental variations. Since there were more than three groups of experiments, the differences in echogenicity among groups were analyzed by one-way ANOVA and Tukey tests for multiple comparisons, with $p < 0.05$ taken as statistically significant. The multiple regression analysis was implemented to model the relationship between echogenicity (the dependent or criterion variable) and different tissue inflammation variables including expression of COX-2, BLT_1, and cell death (the independent or predictor variables). To test the contribution of all candidate variables in echogenicity, the backward elimination procedure was implemented by incorporating all candidates into the model and then testing the deletion of each variable or combinations. The F-test of the overall fit (Prob > F) was chosen with $p < 0.05$ and the adjusted R-Square value (R^2 value) above 0.8 as an observed significance factor to affect echogenicity.

3. Results

3.1. Echogenicity discloses tissue changes at the early stage of fracture

The B-mode images were acquired from the medial legs of mice using an ultrasound with frequency close to 50 MHz, in which a typical image is given in Fig. 1C. The detail features

for the soft tissue of mouse legs, such as muscle features and fascicles, were discerned (Fig. 2, left panel). Both the tibia and fibula bones tended to cause shading effects in the ultrasound images. The ultrasound images revealed changes of tissue composition in the soft tissue near the fractured bone. The ultrasonography and Nakagami distribution of ultrasound signals acquired from tissues before fracture injury, immediately after fracture (D0), and on post-fracture days 2, 4, and 7 (Fig. 2) were used to characterize changes of tissue properties. During the healing progression, the swelling in mouse leg tissues caused a simultaneous increase in both echogenicity of the soft tissue near fractured bone and the depth of subcutaneous tissue. To further quantify the dynamic changes in echogenicity and Nakagami distribution, the ROI near the fractured bone was selected to document soft tissue inflammation and compare it to the control region of the same mouse. The selected ROIs in the ultrasonogram were marked by a white square (left panel) and those of the corresponding Nakagami images were marked by a red square (right panel) (Fig. 2). The echogenicity of ultrasound images was observed to increase at different time points, and those of corresponding Nakagami parameters with values of near one did not vary significantly. The unified values of Nakagami parameters in the ROIs suggested that the corresponding tissue properties were homogeneous.

The gray-scale echogenicity of multiple bone-fractured mouse ROIs at different time points were further analyzed. Results calculated from different sizes of ROIs, including 80 × 60, 60 × 45, and 40 × 30 pixels, demonstrated a similar tendency of the increase in echogenicity (Fig. 3A). The ultrasound image showed not only an increase of mean echogenicity but also an increase in the variation of gray values, with a shift in the distribution (between 25% and 75% of whole population) from around 20–45 to 40–80 of gray values (Fig. 3A). This result suggested the tissue inflammation triggered by bone fracture is responsible for the increase of echogenicity for most of the pixels within the ROI. The rationale in determining the ROI size was to assure that a sufficiently large region of the inflamed soft tissue is documented but to exclude the bone tissue and skin. This study determined that a ROI of 80 × 60 pixels, estimated to be 856 × 642 μm approximately, was appropriate and applicable for the calculation of echogenicity and statistical parameter.

The inflammatory process involved in mouse leg bone repair is three-dimensional (3D) in nature. Since a sequence of ultrasound images was acquired from each scanning, it allows measurement of the echogenicity from several cross-sections (about 500 μm) near the selected ROIs images (Fig. 3B). In comparison the increase of echogenicity from the post-fracture day two (gray scale around 45) with that of day seven (gray scale around 65), only a minor change (less than 10 in gray scale) within several cross-sections (about 500 μm) is observed (Fig. 3B). Thus, the uniform increase of gray scale during early inflammation was confirmed.

3.2. Dynamic monitoring of echogenicity and correlation of tissue inflammation with hyperechogenic ultrasonogram

Dynamic changes of echogenicity of tissues were detected by ultrasound at a frequency close to 50 MHz before fracture injury, immediately after fracture (D0), and on post-fracture days 2, 4, 7, and 14 (Fig. 4). The dynamic change was quantified by normalizing the

echogenicity calculated from the selected ROIs of the fractured mice to those of the same ROI before fracture. The echogenicity significantly increased on four (1.43 ± 0.12 folds) and seven (1.76 ± 0.17 folds) days post fracture, but decreased on post-fracture day of 14 (1.09 ± 0.1 folds).

The histology studies were performed to correlate variations of tissue structures with the corresponding echogenicity obtained from the 50 MHz ultrasound images. Mice were immediately sacrificed after the completion of each ultrasound measurements, and then histological staining (H&E) was carried out (Fig. 5A). Before fracture, the intact contours of subcutaneous vessels and individual muscle groups could be clearly identified in both histographic and ultrasonic images. Two days post fracture, both ultrasound and H&E staining images showed skin and subcutaneous tissue hypertrophy, damage of muscle tissue, and discontinuity of bone contours. Hematomas were formed in the lesion tissue, which correlated to the increase of gray levels or hyperechogenicicty in ultrasonic images on post-fracture days of four and seven (Fig. 5A).

Further assessments of histological samples revealed the status of tissue damage and inflammation in the fractured leg. Soft tissue in the posteromedial compartment near the fractured tibia corresponding to the locations of ultrasound measurements were stained with H&E, TUNEL, and COX-2 (Fig. 5B). The ROI (square in Fig. 5A) in the referred areas, showed the destruction of muscle tissue in magnified H&E images taken on post-fracture days of two and four (Fig. 5B. 1st panel). H&E staining showed chondrocyte-like cells and soft callus formation after fracture for seven days. Cell death on days 2, 4, and 7 after fracture were identified by positive staining of cell nuclei with TUNEL assay (red arrow) (Fig. 5B. 2nd panel). A significant increase in cell apoptosis occurred on post-fracture day two and minimally decreased on post-fracture days four and seven. IHC staining of COX-2 revealed increases in COX- 2 positive cells (red arrow) on post-fracture days four and seven (Fig. 5B. 3rd panel). Another inflammatory mediator, BLT_1, also increased on post-fracture days four and seven (Fig. 5B. 4th panel). TUNEL, COX-2, and BLT_1 staining of inflamed tissue showed positive cells with brown coloring in the cell nuclei (Fig. 5, red arrow). The percentage of positive cells for TUNEL, COX-2, and BLT_1 were quantified from at least three animals under the same experimental conditions (Fig. 5C). Multiple regressions showed several significant combinations that could contribute to the echogenicity (Table 2, $p < .05$). By using the backward elimination procedure for identifying the excludable variable, the only combination cannot reflect echogenicity variation was the condition that eliminated COX-2 (Table 2, $p = 0.099$ and adjusted $R^2 = .954$ when only use TUNEL + BLT_1). By considering the maximum value of adjusted R-square (Max. Adj. R^2), the multiple regression results suggested the optimal indicators correlated to the increase of echogenicity after fracture were the combination of TUNEL and COX-2 positive cells (Table 2, adjusted R^2=.963 with bold and underline text). The regression results also suggested the echogenicity could indicate the existence of tissue inflammation by using individual variables of TUNEL, COX-2, and BLT_1 (Table 2, $p < .05$). Thus, the areas with increasing echogenicity in ultrasound images may correlate to the induction of tissue inflammation after bone fracture. Among each individual variable, COX-2 showed the best

fitted result to explain the changes in echogenicity (adjusted R^2 = .954 when fitting COX-2 and echogenicity).

3.3. Echogenicity records the dynamic responses to various nonsteroidal anti-inflammatory drug treatments after fracture

Commonly used inflammation inhibitors were selected to study the effects of NSAID treatments on inflammation. Mice were orally fed Asp, IND, and SC-236 daily for seven days and monitored by echogenicity on D0, 2, 4, and 7 since inflammation and echogenicity decreased to base line on post-fracture day 14. A change of ultrasound echogenicity suggested that treatment with any of the inflammatory inhibitors may influence early fracture healing responses (Fig. 6). Significant increases of echogenicity (*, $p < .05$) were observed in mice without receiving drug treatment as well as in those fracture mice administered IND and SC-236. Those mice treated with IND showed an early occurrence of increasing echogenicity, on the post-fracture day two (1.45 ± 0.29 folds), and enhancing less prominent increase of echogenicity on post-fracture day four (IND treatment: 1.55 ± 0.17 folds and without drug treatment: 1.41 ± 0.16 folds). Similar to the fracture mice without receiving treatment, the administration of SC-236 did not result in observable echogenicity changes at any time. Asp treated mice showed no obvious change in echogenicity at different time points. On post-fracture day 7, a significant decrease of echogenicity (1.14 ± 0.29 folds) was found between the Asp-treated mice and the mice without treatment (1.71 ± 0.21 folds) (&, $p < .05$).

Further specific immunohistological staining was performed to validate tissue inflammation by the assessments of TUNEL, COX-2, and BLT_1 relative to those of ultrasound measurements (Fig. 7A). On day 7 after fracture, the TUNEL, COX-2, and BLT_1 staining of inflamed tissues showed positive cells with brown coloring in the cell nuclei in the mice without NSAID treatments. The percentage of positive cells for TUNEL, COX-2, and BLT_1 were quantified from at least three animals of the same experimental condition (Fig. 7B). The Asp treatment significantly inhibited cell apoptosis and expression of COX-2 and BLT_1. The IND-treated mice showed a decrease of BLT_1 expression, but exhibited no significant changes in cell apoptosis ($p > .05$) or COX-2 expression ($p > .05$) when compared to fractured mice without treatment. Similarly, treatment with SC-236 slightly reduced COX-2 expression in the tissue of fracture mice, but did not alter cell apoptosis or BLT_1 expression. These results suggest that either COX-2 or 5-LO activate inflammatory responses, causing cell apoptosis and increasing echogenicity of ultrasound images. The daily treatment of Asp prevented inflammation after bone fracture and this may be detected from ultrasound images. This is further supported by the reduction of inflammatory responses among cell apoptosis, and COX-2 and BLT_1 expressions.

4. Discussion

In the present study, a non-invasive approach using ultrasound of a center frequency near 50 MHz is demonstrated to be feasibly able to assess tissue inflammation in living animals. Ultrasound is free of radioactivity that is capable of providing an immediate visualization of structural changes to monitor fracture healing. A previous study using 5 MHz ultrasound had demonstrated the ability to monitor fracture healing processes in humans [33].

Hypoechogenicity was found in the areas over the bone gap during the hematoma phase and also upon the initiation of the soft callus formation phase. However, the external callus tissue formed within muscle tissue appeared as hyperechoic areas in the case of acute peri-fracture hematomas. These hyperechoic areas gradually varied to hypoechoic areas between post-fracture days of 7 and 28 [34]. The fracture healing process involves tissue transformation that may change the acoustic characteristics in soft tissue and subsequently result in echogenic enhancement. Previous studies investigated the fracture healing either only by ultrasound or histological assessment, this current study provide the monitor of progressive changes in ultrasound echogenicity and simultaneously correlation to inflammatory responses on the same animal between post-fracture days of 2 and 14 (Fig. 2). In addition to the time-course monitoring of inflammation in both soft and hard tissues of whole mouse leg sections, the use of 50 MHz ultrasound is capable of achieving sufficient resolution to correlate with histological analysis. However, the remodeling processes in the later phase of bone healing might limit the ultrasonic applications of current study. After the acute inflammatory phase, the continuous deposition of extracellular matrix by chondrocyte-like cells may influence the echogenicity when forming a callus after 14-days post fracture. To further estimate hard tissue properties, the sound velocity of hard tissues was measured and a decreased velocity in the bone was demonstrated after osteotomy on sheep tibia which progressively increased during the healing progresses [35]. The combination of ultrasound imaging with elastography may further benefit the understanding of tissue properties and healing processes after acute inflammation.

The ultrasonic results obtained from the mouse-tibia fracture model successfully demonstrated that it is feasible to monitor the healing processes of the fracture, which is similar to results found in previous studies [24]. In mouse studies, tibia fractures show initiation of new bone formation by day seven, peak callus cartilage formation by post-fracture day nine, and bone union with 75% of original strength by day twenty-eight [24]. The fracture healing process in human tibia usually requires more time, with an average 43–49 weeks to complete recovery [36]. In the hematoma phase, inflammatory cells infiltrate the fracture site where they combat infection [2]. On the post-fracture day two, dead tissue and infiltrated immune cells occupy the fracture site. During soft callus formation, tissue is dominated by chondrocytes and fibroblasts [2]. Hiltunen et al. identified the occurrence of cartilage- like areas on the post-fracture day five in fractured mice [24]. These areas contained mesenchymal tissue, which showed significant expression on the post-fracture day seven and then gradually decreased until the post-fracture day 28 [24]. The chondrocyte-like and fibroblast-like cells during the soft callus formation phase between post-fracture days of four and seven were also observed in current study (Fig. 5A). According to immunohistological results, bone fracture induced the expressions of both COX-2 and BLT_1 (Fig. 5B). The initiation of COX-2 on the post-fracture day four and its significant presentation on day seven were also in agreement with previous reports [37]. The expression of BLT_1 in tissue surrounding fractured bone was verified by results of current and previous studies [11]. In addition to the histological analysis of soft tissue composition (Fig. 5A) and immunohistological evidence of inflammatory proteins (Fig. 5B) found in current study, the inflammatory responses in soft tissues were correlated to the hyperechogenicity of these tissues in ultrasound images (Table 2). The multiple regressions results (Max. Adj. R^2)

suggested that the hyperechogenic images could indicate the TUNEL and COX-2 positive cells (Table 2).

NSAIDs are consisted of a group of compounds of diverse chemical structures distinct from corticosteroids, but they possess common steroid-like anti-inflammatory actions [38]. Recent reports have indicated that the use of NSAIDs may be associated with the risk of myocardial infarction [39]. Induction of endothelial cell apoptosis by perturbing the peroxisome proliferator-activated receptor delta transcriptional pathway was discovered in the treatments of IND and selective COX-2 inhibitors, but not Asp [40]. Recently in previous *in vitro* study, we demonstrated that treating human osteoblasts with IND under hypoxic conditions resulted in increased cell death and a decrease of alkaline phosphatase activity [41]. Asp is also commonly used in clinics, and it however boosts the damage of osteoblasts at the cellular level when subjected to hypoxic condition [41]. In this current study, the reduction of tissue inflammation in fractured mice demonstrated from histology was positively correlated to those of ultrasonic findings. It thus is possible to monitor the responses of NSAID treatments in living animals with ultrasound non-invasively (Fig. 6). The remodeling processes at the tissue level involve chemical and mechanical activations, and interactions including intracellular signal activations, cell-cell interactions and cell-matrix interactions [42]. Therefore, dynamic monitoring of the responses during NSAID treatments could provide a non-invasive platform to reveal the tissue remodeling in the future.

There are other factors necessary to be considered in future implementations of ultrasound modality. Because the bone fracture resulted in the swelling of tissue section, the selections of ROI were based on the position relatively to the anatomical landmark. The current method to select the ROI by relating to an anatomical landmark is subjective, and might result in a small shift of several pixels depending on the chosen location. Nevertheless, this minor variation did not significantly alter the tendency of estimated echogenicity. The hematoma tissue showed homogeneous composition that further supported the even distribution of tissue property during the inflammation stage after tibia fracture. In addition, each experimental condition was repeated in at least three animals and those results showed a remarkable consistency with a standard deviation of less than 10% (Fig. 4). It was found that the ROI with a size of 80 × 60 pixels is suitable for the purpose of current study. The smaller size ROIs, such as 60 × 45 and 40 × 30 pixels, may cause under-sampling of data. This statement is supported by the IHC data when counting the positive inflammatory cells within the ROI of IHC staining images (Fig. 5). The volume of inflammatory tissue may also an important factor in indicating the inflammation level. The identification of inflammatory tissue boundary from ultrasound images and 3D reconstruction of tissue structures will be studied in the future. In current study, the echogenicity and Nakagami parameters were used to investigate the ultrasound parameter in fracture healing. The tissue inflammation was correlated to the increase of echogenicity. Although Nakagami parameters did not associate to the inflammatory responses, the constant value in Nakagami parameters suggested the homogeneous properties in the corresponding tissue. Other ultrasound quantitative parameters, such as integrated backscatter (IB) that indicates the average intensity of ultrasonic backscattering signals, may also be applied to explore tissue healing.

There are some limitations when using 50 MHz ultrasound to monitor the fracture healing. The penetration depth of 50 MHz ultrasound, approximately 5 mm, may limit the use of the current approach in humans. The ultrasound fracture diagnosis model was based on the tibia of mice in this study. The bone fractures covered by less thick skin and subcutaneous tissue, such as the forearm, wrist, fingers, leg, ankle, foot, and skull, are feasible to be studied by 50 MHz ultrasound. However, the axial skeleton and long bones covered by multiple layers of muscles remain difficult to explore by the current approach. There are other pro-inflammatory protein molecules secreted after tissue damage, such as transforming growth factor β, tumor necrosis factor α, interferon γ, interleukin 10 and 12 [43,44]. These inflammation factors may not only regulate inflammatory signal cascades, but also participate in modulating tissue regeneration. Further research will investigate the involvement of other inflammatory factors detectable by ultrasound.

5. Conclusion

The current study successfully utilized a mouse fracture model to investigate tissue inflammation responses within 2 weeks of healing process after fracture injury using ultrasound at 50 MHz high frequency. The ultrasound images showed that hyperechogenity is positively correlated with inflammatory responses from the tissues surrounded the fractured bone. Dynamic changes in tissue inflammation during treatment with several different NSAIDs were determined from the echogenicity in ultrasound images. Among the various NSAIDs, ultrasound imaging showed that Asp effectively inhibited the inflammatory response in fracture mice, resulting in a decreased echogenicity when compared to the fractured mice without drug treatment. These results suggest that ultrasound may provide a non-invasive means to study tissue inflammation and interactions between inflammation and therapeutic strategies in living animals. By elucidating the dynamics of tissue inflammatory responses, detailed molecular interactions and cell responses may be elucidated to benefit bone healing. The current study has the potential to be applied to diseased mouse models presenting with bone healing problems, such as osteoporosis.

Acknowledgments

The authors thank for the funding supports from National Health Research Institute (Taiwan) by Grant NHRI-EX101-10115EC and in part by National Science Council (Taiwan) Grants NSC 99-2320-B-006-002-MY3 and NSC 98-2627-B-006-010-MY3. The authors are very grateful to Dr. Michael W. Hughes for valuable suggestions.

Abbreviations

3D	three-dimensional
5-LO	5-lipoxygenase
AA	arachidonic acid
Asp	aspirin
BLT_1	Leukotriene B4 receptor 1
COX	cyclooxygenase

COX-2	cyclooxygenase-2
DAB	3,3′-Diaminobenzidine
ddH_2O	double distilled H_2O
EtOH	ethanol
FBS	fetal bovine serum
IACUC	Institutional Animal Care and Use Committee
IB	integrated backscatter
IHC	immunohistochemistry
IND	indomethacin
H&E	Hematoxylin and eosin
Max. Adj. R^2	maximum value of adjusted *R*-square
MRI	Magnetic resonance imaging
NCKU	National Cheng Kung University
NSAIDs	non-steroidal anti-inflammatory drugs
PGE2	prostaglandin E2
R^2 value	*R*-square value
RF	radio-frequency
ROI	region of interest
SD	standard deviation
STIR	Short TI Inversion Recovery
TBST	Tris-buffered saline with tween 20
TUNEL	deoxynucleotidyl transferase dUTP nick end-labeling

References

1. Remedios A. Bone and bone healing. Vet Clin North Am Small Anim Pract. 1999; 29:1029–1044v. [PubMed: 10503283]
2. Schindeler A, McDonald MM, Bokko P, Little DG. Bone remodeling during fracture repair: the cellular picture. Semin Cell Dev Biol. 2008; 19:459–466. [PubMed: 18692584]
3. Marsell R, Einhorn TA. The biology of fracture healing. Injury. 2011; 42:551–555. [PubMed: 21489527]
4. Xie C, Ming X, Wang Q, Schwarz EM, Guldberg RE, O'Keefe RJ, Zhang X. COX-2 from the injury milieu is critical for the initiation of periosteal progenitor cell mediated bone healing. Bone. 2008; 43:1075–1083. [PubMed: 18773980]
5. Kolar P, Schmidt-Bleek K, Schell H, Gaber T, Toben D, Schmidmaier G, Perka C, Buttgereit F, Duda GN. The early fracture hematoma and its potential role in fracture healing. Tissue Eng Part B Rev. 2010; 16:427–434. [PubMed: 20196645]
6. Abdul-Hadi O, Parvizi J, Austin MS, Viscusi E, Einhorn T. Nonsteroidal antiinflammatory drugs in orthopaedics. J Bone Joint Surg Am. 2009; 91:2020–2027. [PubMed: 19651965]

7. Kawabata A. Prostaglandin E2 and pain – an update. Biol Pharm Bull. 2011; 34:1170–1173. [PubMed: 21804201]
8. Murphy RC, Gijon MA. Biosynthesis and metabolism of leukotrienes. Biochem J. 2007; 405:379–395. [PubMed: 17623009]
9. Marcouiller P, Pelletier JP, Guevremont M, Martel-Pelletier J, Ranger P, Laufer S, Reboul P. Leukotriene and prostaglandin synthesis pathways in osteoarthritic synovial membranes: regulating factors for interleukin 1beta synthesis. J Rheumatol. 2005; 32:704–712. [PubMed: 15801029]
10. Cottrell JA, O'Connor JP. Pharmacological inhibition of 5-lipoxygenase accelerates and enhances fracture-healing. J Bone Joint Surg Am. 2009; 91:2653–2665. [PubMed: 19884440]
11. Manigrasso MB, O'Connor JP. Accelerated fracture healing in mice lacking the 5-lipoxygenase gene. Acta Orthop. 2010; 81:748–755. [PubMed: 21067431]
12. Dimmen S, Nordsletten L, Madsen JE. Parecoxib and indomethacin delay early fracture healing: a study in rats. Clin Orthop Relat Res. 2009; 467:1992–1999. [PubMed: 19319614]
13. Brown KM, Saunders MM, Kirsch T, Donahue HJ, Reid JS. Effect of COX-2-specific inhibition on fracture-healing in the rat femur. J Bone Joint Surg Am. 2004; 86-A:116–123. [PubMed: 14711953]
14. Dimmen S, Nordsletten L, Engebretsen L, Steen H, Madsen JE. Negative effect of parecoxib on bone mineral during fracture healing in rats. Acta Orthop. 2008; 79:438–444. [PubMed: 18626809]
15. Gerstenfeld LC, Thiede M, Seibert K, Mielke C, Phippard D, Svagr B, Cullinane D, Einhorn TA. Differential inhibition of fracture healing by nonselective and cyclooxygenase-2 selective non-steroidal anti-inflammatory drugs. J Orthop Res. 2003; 21:670–675. [PubMed: 12798067]
16. Ring EF, Ammer K. Infrared thermal imaging in medicine. Physiol Meas. 2012; 33:R33–46. [PubMed: 22370242]
17. Schulze M, Kotter I, Ernemann U, Fenchel M, Tzaribatchev N, Claussen CD, Horger M. MRI findings in inflammatory muscle diseases and their noninflammatory mimics. AJR Am J Roentgenol. 2009; 192:1708–1716. [PubMed: 19457839]
18. Shung, KK. Diagnostic ultrasound: imaging and blood flow measurements. Taylor & Francis Group; New York: 2006.
19. Lin YH, Huang CC, Wang SH. Quantitative assessments of burn degree by high-frequency ultrasonic backscattering and statistical model. Phys Med Biol. 2011; 56:757–773. [PubMed: 21239847]
20. Kim HH, Cannata JM, Liu R, Chang JH, Silverman RH, Shung KK. 20 MHz/40 MHz dual element transducers for high frequency harmonic imaging. IEEE Trans Ultrason Ferroelectr Freq Control. 2008; 55:2683–2691. [PubMed: 19126492]
21. Cannata JM, Ritter TA, Chen WH, Silverman RH, Shung KK. Design of efficient, broadband single-element (20–80 MHz) ultrasonic transducers for medical imaging applications. IEEE Trans Ultrason Ferroelectr Freq Control. 2003; 50:1548–1557. [PubMed: 14682638]
22. Knspik DA, Starkoski B, Pavlin CJ, Foster FS. A 100–200 MHz ultrasound biomicroscope. IEEE Trans Ultrason Ferroelectr Freq Control. 2000; 47:1540–1549. [PubMed: 18238700]
23. Duckett AS, Reid AD, Leamen L, Cucevic V, Foster FS. Thermal assessment of 40-MHz ultrasound at soft tissue-bone interfaces. Ultrasound Med Biol. 2004; 30:665–673. [PubMed: 15183233]
24. Hiltunen A, Vuorio E, Aro HT. A standardized experimental fracture in the mouse tibia. J Orthop Res. 1993; 11:305–312. [PubMed: 8483044]
25. Burckhardt CB. Speckle in ultrasound B-mode scans. IEEE Trans Son Ultrason. 1978; 25:1–6.
26. Wagner RF, Insana MF, Brown DG. Statistical properties of radio-frequency and envelope-detected signals with applications to medical ultrasound. J Opt Soc Am A, Opt Image Sci. 1987; 4:910–922.
27. Weng L, Reid JM, Shankar PM, Soetanto K. Ultrasound speckle analysis based on the K distribution. J Acoust Soc Am. 1991; 89:2992–2995. [PubMed: 1918635]
28. Dutt V, Greenleaf JF. Ultrasound echo envelope analysis using a homodyned K distribution signal model. Ultrason Imaging. 1994; 16:265–287. [PubMed: 7785128]

29. Shankar PM. A model for ultrasonic scattering from tissues based on the K distribution. Phys Med Biol. 1995; 40:1633–1649. [PubMed: 8532745]
30. Shankar PM. Ultrasonic tissue characterization using a generalized Nakagami model. IEEE Trans Ultrason Ferroelectr Freq Control. 2001; 48:1716–1720. [PubMed: 11800135]
31. Tsui PH, Chang CC. Imaging local scatterer concentrations by the Nakagami statistical model. Ultrasound Med Biol. 2007; 33:608–619. [PubMed: 17343979]
32. Serhan CN, Savill J. Resolution of inflammation: the beginning programs the end. Nat Immunol. 2005; 6:1191–1197. [PubMed: 16369558]
33. Ricciardi L, Perissinotto A, Dabala M. Mechanical monitoring of fracture healing using ultrasound imaging. Clin Orthop Relat Res. 1993:71–76. [PubMed: 8339511]
34. Maffulli N, Thornton A. Ultrasonographic appearance of external callus in long-bone fractures. Injury. 1995; 26:5–12. [PubMed: 7868211]
35. Protopappas VC, Baga DA, Fotiadis DI, Likas AC, Papachristos AA, Malizos KN. An ultrasound wearable system for the monitoring and acceleration of fracture healing in long bones. IEEE Trans Biomed Eng. 2005; 52:1597–1608. [PubMed: 16189973]
36. Keating JF, Blachut PA, O'Brien PJ, Court-Brown CM. Reamed nailing of Gustilo grade-IIIB tibial fractures. J Bone Joint Surg Br. 2000; 82:1113–1116. [PubMed: 11132268]
37. Naik AA, Xie C, Zuscik MJ, Kingsley P, Schwarz EM, Awad H, Guldberg R, Drissi H, Puzas JE, Boyce B, Zhang X, O'Keefe RJ. Reduced COX-2 expression in aged mice is associated with impaired fracture healing. J Bone Miner Res. 2009; 24:251–264. [PubMed: 18847332]
38. Simon LS, Mills JA. Drug therapy: nonsteroidal antiinflammatory drugs (first of two parts). New Engl J Med. 1980; 302:1179–1185. [PubMed: 6988717]
39. Chan AT, Manson JE, Albert CM, Chae CU, Rexrode KM, Curhan GC, Rimm EB, Willett WC, Fuchs CS. Nonsteroidal antiinflammatory drugs, acetaminophen, and the risk of cardiovascular events. Circulation. 2006; 113:1578–1587. [PubMed: 16534006]
40. Liou JY, Wu CC, Chen BR, Yen LB, Wu KK. Nonsteroidal anti-inflammatory drugs induced endothelial apoptosis by perturbing peroxisome proliferator-activated receptor-delta transcriptional pathway. Mol Pharmacol. 2008; 74:1399–1406. [PubMed: 18678619]
41. Liu C, Tsai AL, Chen YC, Fan SC, Huang CH, Wu CC, Chang CH. Facilitation of human osteoblast apoptosis by sulindac and indomethacin under hypoxic injury. J Cell Biochem. 2012; 113:148–155. [PubMed: 21882223]
42. Su FC, Wu CC, Chien S. Review: roles of microenvironment and mechanical forces in cell and tissue remodeling. J Med Biol Eng. 2011; 31:233–244.
43. Soleymaninejadian E, Pramanik K, Samadian E. Immunomodulatory properties of mesenchymal stem cells: cytokines and factors. Am J Reprod Immunol. 2012; 67:1–8. [PubMed: 21951555]
44. Harder AT, An YH. The mechanisms of the inhibitory effects of nonsteroidal anti-inflammatory drugs on bone healing: a concise review. J Clin Pharmacol. 2003; 43:807–815. [PubMed: 12953337]

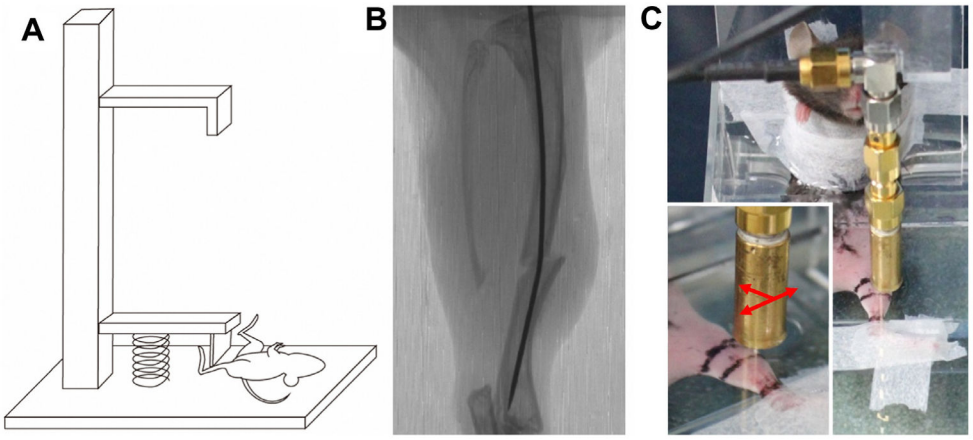

Fig. 1.

A free-dropping impacted-injury simulator was used to create a fracture on the middle shaft of mice tibia (A). Immediately after injury, an X-ray was taken to confirm complete fracture (B). A custom-made plexiglass restrainer was used to confine the position of mice during ultrasound scanning (C). A swept scanning was performed on the longitudinal axis of fractured tibia from distal to proximal leg (arrow).

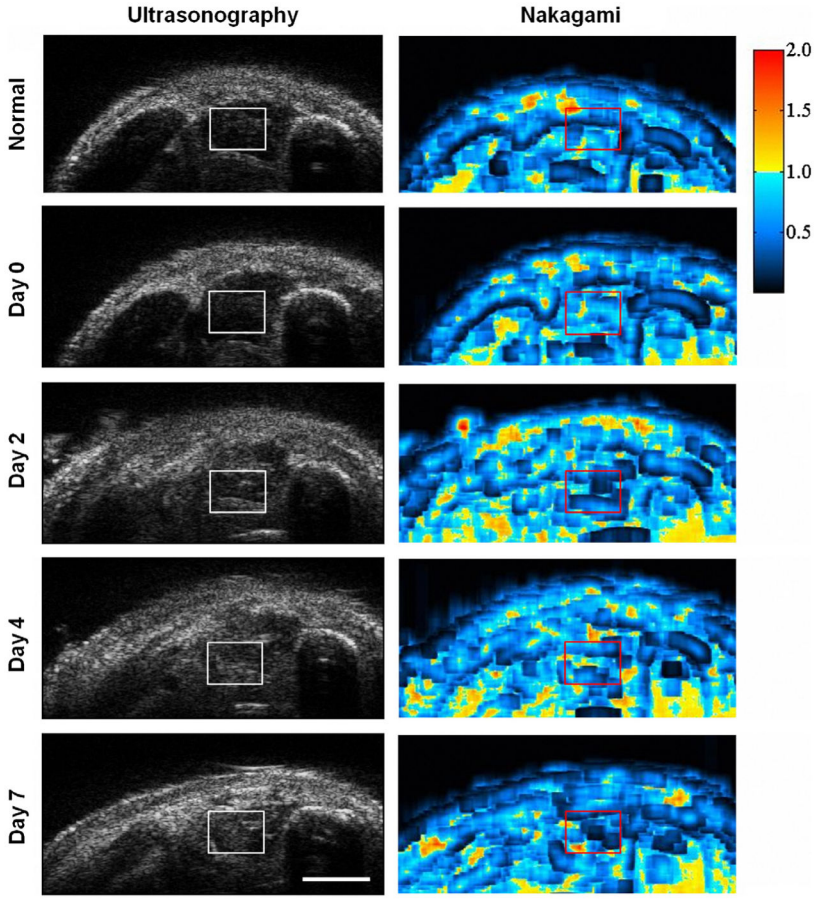

Fig. 2.

Complete fractures were created on the middle shaft of tibia in mice. 48 MHz ultrasound images were obtained in the same mice before fracture, immediately after the fracture injury (post-fracture day 0), and on post-fracture days 2, 4, and 7 (left panel). The distributions of scattering properties for the tissue after fracture were demonstrated by Nakagami distribution (right panel). The region of interest was labeled in square with the prefer size of 80 × 60 pixels. Bar = 1 mm.

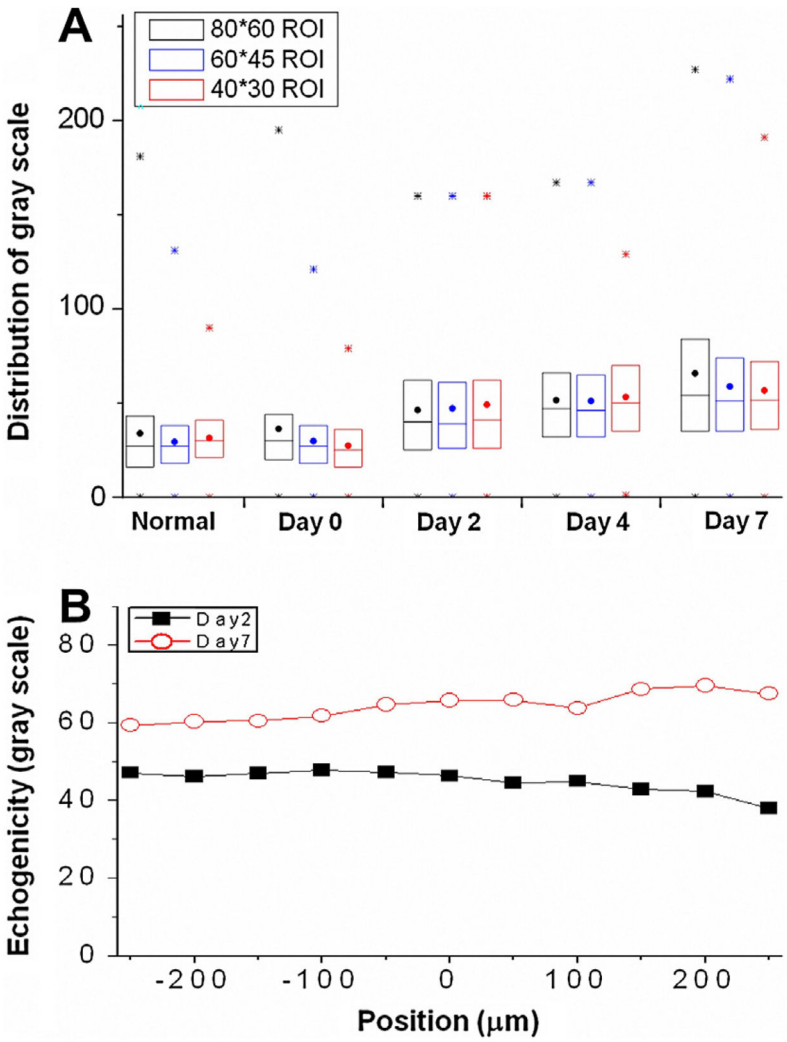

Fig. 3.

The distributions for the gray-scale in the region of interest (ROI) were demonstrated by the max/min (*), the range of 75–50–25% (box), and mean value (.) (A). The increases of gray scale in major population were observed regardless of ROI sizes after fracture. To further confirm the distribution of tissue properties in three dimension, the echogenicity in different cross-sections distal (negative scale) and proximal (positive scale) to the selected plane (position = 0) used in current study were qualified by using the same reference position of ROI (B). As comparing to the difference of echogenicity observed between post-fracture day 2 and 7, the small changes of echogenicity within the range of 500 μm suggested the homogenous tissue properties within the inflammatory area.

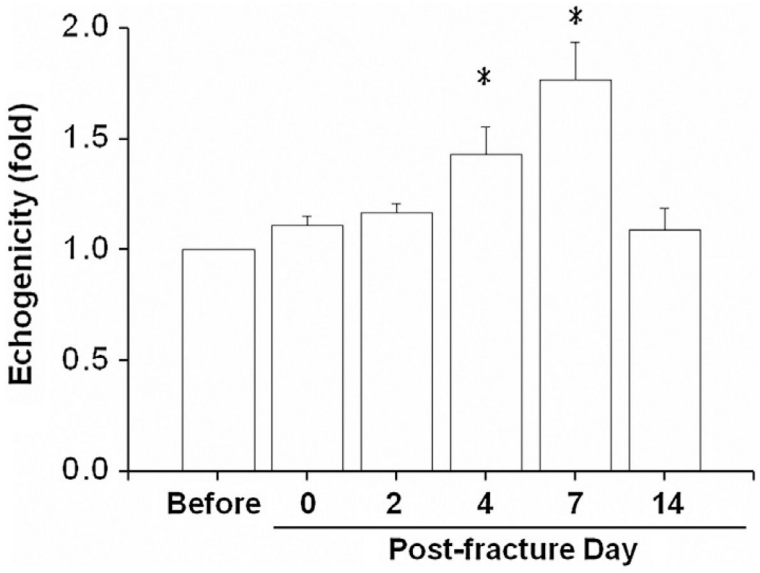

Fig. 4.

Dynamic changes in echogenicity in the soft tissue posteromedial to the fracture site in a frame of the region of interest (ROI) were quantified from ultrasonic images. Significant increases in echogenicity were measured for four and seven days post fracture. *: significant difference ($P < .05$) from the referred ROI before fracture.

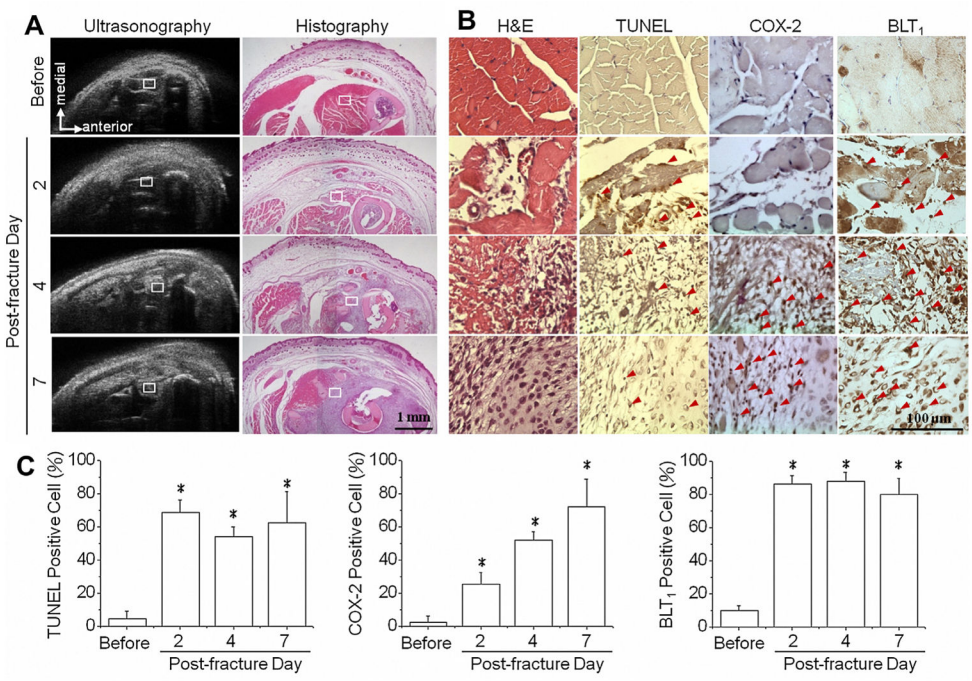

Fig. 5.

Histological studies were performed to investigate structural changes and to correlate inflammation patterns to the region of interest (ROI) observed in ultrasonic images. Mice were sacrificed immediately after ultrasound scanning and obtained different time points before fracture, and on post-fracture days 2, 4, and 7. Hematoxylin and eosin (H&E) staining demonstrated the morphological and compositional changes in lesion tissue, which closely correlated with ultrasonography results (A). The ROIs in ultrasonic images were further assessed by *in situ* terminal deoxynucleotidyl transferase dUTP nick end-labeling (TUNEL) assay and immunohistological staining of cyclooxygenase-2 (COX-2) and Leukotriene B4 receptor 1 (BLT_1) proteins (B). The percentages of positive cells were quantified by counting positive stained nucleus and divided to the total cell number in ROI (C). The increase of cell apoptosis with presentation of both COX-2 and BLT_1 (red arrow) confirmed the tissue inflammation after fracture injury. *: significant difference ($P < .05$) from the referred ROI before fracture. Bar in ultrasonographic image = 1 mm. Bar in immunohistochemistry image = 100 μm. (For interpretation of the references to colour in this figure legend, the reader is referred to the web version of this article.)

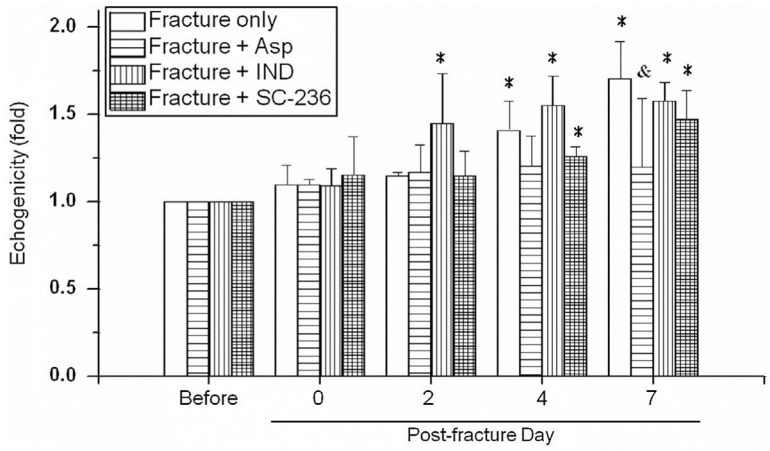

Fig. 6.

Dynamic changes in echogenicity after administering different anti-inflammatory drugs to the same fracture mice were observed by daily feeding the aspirin (Asp), indomethacin (IND), or selective COX-2 inhibitor (SC-236). Asp treatment prohibited fracture-induced echogenicity on post-fracture day seven. Ultrasonographic of IND treated mice promoted the occurrence of hyperechogenic image at two days post fracture. *: significant difference ($P < .05$) from the referred ROI before fracture. &: significant difference ($P < .05$) from the referred ROI in the time-matched fracture mice without drug treatment.

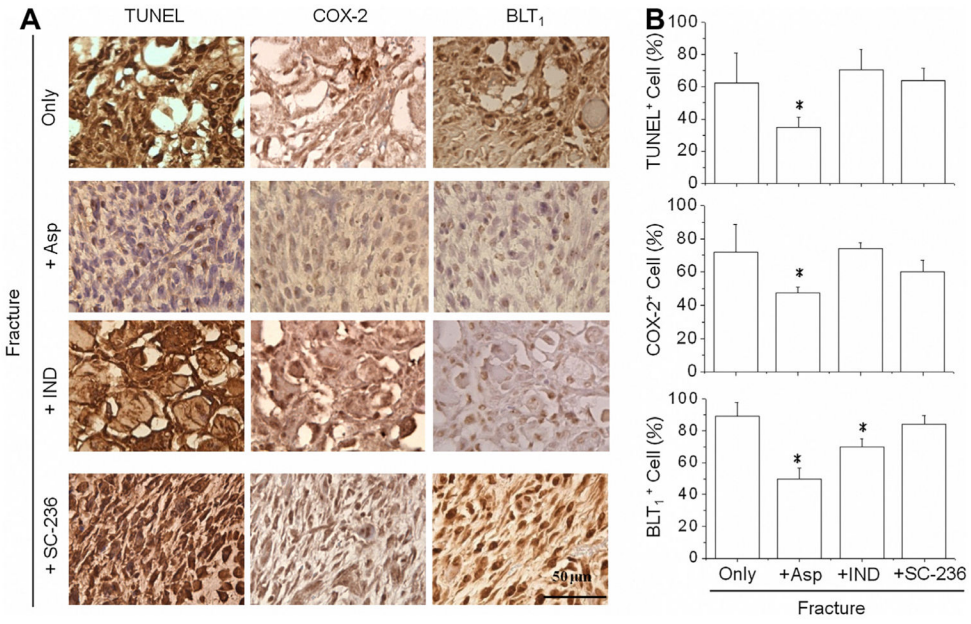

Fig. 7.

The region of interests (ROI) in ultrasonic images were further assessed by TUNEL, COX-2, and BLT_1 staining to correlate the inflammatory patterns (A). The percentages of positive cells were quantified by counting positive stained nucleus and divided to the total cell number in ROI (B). Reductions in the number of positive cells for TUNEL, COX-2, and BLT_1 staining were found in mice treated with aspirin which is highly agreed with the echogenicity in Fig. 6. Histological evidences for other antiinflammatory drugs also demonstrated that inhibition of either COX-2 or BLT_1 alone is insufficient to reduce cell apoptosis and decrease tissue inflammation after fracture injury. *: significant difference ($P < .05$) from the referred region without treatment. Bar = 50 μm.

Table 1

Characteristics of transducer.

Central frequency	48 MHz
−6 dB bandwidth	35 MHz
f-number	1.5
Depth of focus	6 mm
Aperture size	4 mm
Axial resolution	24 μm
Lateral resolution	48 μm

Table 2

Multiple regressions showed several inflammatory factors were correlated to the increases of echogenicity in the mice after tibia fracture (*, $p < .05$). The contribution of different candidate variables in echogenicity was examined by the backward elimination of each variable or combinations. The adjusted *R*-square (Adj. R^2) suggested the best combination to reflect the hyperechogenic ultrasonography in fractured bone was the positive cells in TUNEL and COX-2 immunostaining (underline Adj. $R^2 = 0.963$).

Contribution variables	Deleted factor	Adj. R^2	*P* value
TUNEL + COX-2 + BLT_1		0.959	<0.01*
TUNEL + COX-2	BLT_1	<u>0.963</u>	<0.01*
TUNEL + BLT_1	COX-2	0.268	0.099
COX-2 + BLT_1	TUNEL	0.959	<0.01*
TUNEL	BLT_1, COX-2	0.335	0.029*
COX-2	BLT_1, TUNEL	0.954	<0.01*
BLT_1	COX-2, TUNEL	0.289	0.041*